Compressional and shear wakes in a two-dimensional dusty plasma crystal

V. Nosenko,* J. Goree,† and Z. W. Ma
Department of Physics and Astronomy, The University of Iowa, Iowa City, Iowa 52242, USA

D. H. E. Dubin
Department of Physics, University of California at San Diego, La Jolla, California 92093, USA

A. Piel
Institut für Experimentelle und Angewandte Physik, Christian-Albrechts Universität, Kiel, Germany
(Received 9 July 2003; published 24 November 2003)

Wakes composed of compressional and shear waves were studied experimentally in a two-dimensional screened-Coulomb crystal. Highly charged microspheres suspended in a plasma settled in a horizontal monolayer and arranged in a triangular lattice with a repulsive interparticle potential. Wakes were excited by a moving spot of Ar^+ laser light. Depending on the laser spot speed, compressional waves formed a Mach cone and multiple lateral or transverse wakes, similar to ship wakes on the water surface, due to a combination of acoustic and dispersive properties. Shear waves, however, formed only a Mach cone, due to their nearly acoustic, i.e., dispersionless character. The experimental results show agreement with a recently developed theory and with molecular dynamics simulations, which assume a binary Yukawa interparticle potential. A generally useful method is presented for calculating the real part of the dispersion relation of the compressional waves based on the analysis of the spatial structure of a phonon wake. Fitting the resulting dispersion relation provides an independent measure of the interparticle potential, parametrized by the screening parameter κ and particle charge Q.

DOI: 10.1103/PhysRevE.68.056409 PACS number(s): 52.27.Lw, 82.70.Dd, 52.35.Fp, 52.27.Gr

I. INTRODUCTION

A moving disturbance can produce waves in a variety of physical systems. Under certain circumstances, they can form a wake pattern, which is stationary as viewed in the moving frame. The structure of this wake depends on the wave characteristics of the medium and the speed and shape of the moving disturbance.

One well-known example of such wakes is the Kelvin wedge that forms behind a ship moving in deep water, shown in Fig. 1. It consists of multiple lateral wakes and transverse wakes. The lateral wakes form an acute angle with the direction of the ship's motion, while transverse wakes are roughly perpendicular to the direction of the ship's motion.

Lateral and transverse wakes arise when waves are dispersive, as they are for a ship's wake on the surface of deep water. A wave is said to be dispersive if its frequency ω is not proportional to wave number k or, equivalently, its phase speed $C=\omega/k$ depends on k.

A Mach cone is another type of wake, which has a single V-shaped structure rather than a multiple structure like the lateral wake of the Kelvin wedge, for example. Mach cones occur in media such as air where the sound speed is the same for all wavelengths. Under these conditions, the wave is said to be dispersionless, obeying an acoustic dispersion relation, $\omega \propto k$.

Waves with a wide range of wave numbers are excited in the near field of a moving disturbance, such as a ship or aircraft, and as they propagate away they interfere with waves that were created at a more distant point when the moving disturbance was there. This interference creates the wake structure that is observed. For a wave that obeys an acoustic dispersion relation, the interference of circular wave fronts occurs on a cone, as shown in Fig. 2(a). This cone has a half angle μ defined by the geometry as

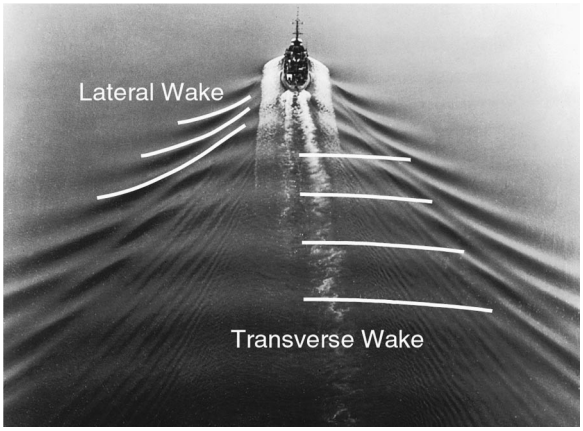

FIG. 1. A Kelvin wedge behind a ship moving in deep water consists of multiple lateral wakes and transverse wakes. This wake structure is due to the dispersion of water waves. To compare, a single Mach cone is formed by dispersionless waves, such as sound waves in air, in a supersonic regime. Photo courtesy of Professor W.H. Munk, Scripps Institute of Oceanography. Reproduced from Fig. 1 of Ref. [37].

*Electronic address: vladimir-nosenko@uiowa.edu
†Electronic address: john-goree@uiowa.edu

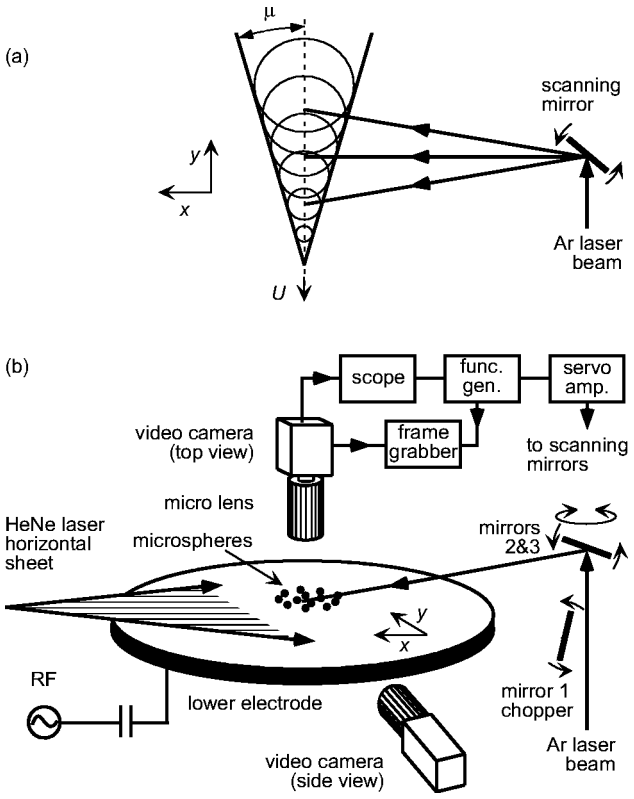

FIG. 2. Experimental apparatus. (a) Phonon wakes are excited in a 2D lattice by the radiation force of a moving laser beam. (b) Polymer microspheres are levitated above the lower electrode in a capacitively coupled rf plasma. The particles settle in a single horizontal layer, arranged in a triangular lattice with hexagonal symmetry.

$$\sin\mu = C_0/U, \tag{1}$$

where U is the speed of the supersonic disturbance and C_0 is the sound speed. The wake in a dispersive medium exhibits a more complicated structure, as we will explore in this paper.

In solids, phonon wakes are of interest in the fields of seismology and materials science. In seismology experiments, Mach cones have been excited in a borehole [1]. Molecular dynamics (MD) simulations of a bcc tungsten crystal with a moving dislocation exhibit a shear-wave Mach cone [2].

Wakes in solids have not been studied as completely as wakes in fluids. Possible reasons include experimental difficulties of making *in situ* measurements in the interior of ordinary solids. Moreover, the time scales in ordinary solids are fast, as determined by the sound speed. In this paper we use a kind of solid that avoids these difficulties.

A dusty plasma crystal is a model system that is well suited for making *in situ* observations of waves and wakes in solids. It is a suspension of micron-size particles in a plasma. The particles are highly charged, and due to mutual repulsion and the plasma's weaker radial electric fields, they arrange themselves in a regular pattern [3–6]. Here we will report results for a two-dimensional (2D) triangular lattice with hexagonal symmetry. The experimental conditions for our particles were similar to those in Ref. [7], where the interparticle potential was experimentally shown to be nearly Yukawa: $U(r)=Q(4\pi\epsilon_0 r)^{-1}\exp(-r/\lambda_D)$, where Q is the particle charge and λ_D is the screening length. The sound speed in this lattice is of the order of a few cm/s and the interparticle spacing is typically $a=0.2$–1 mm. This allows direct imaging of the entire plasma crystal, including its interior, and observation of motion at a microscopic level.

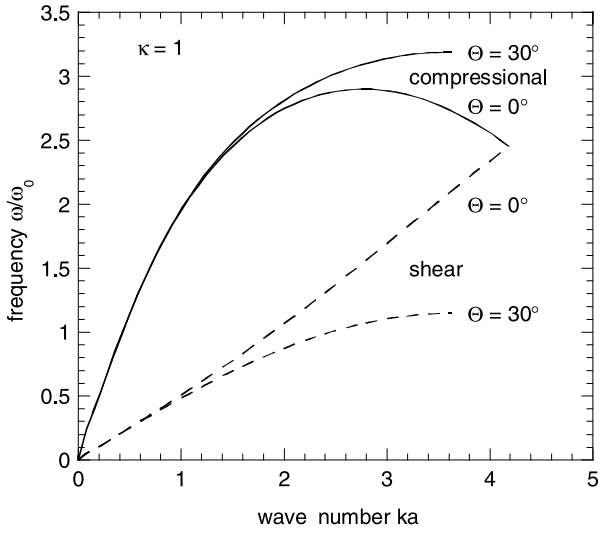

FIG. 3. Theoretical dispersion relation for a 2D triangular Yukawa lattice. It has two modes, compressional and shear. The shear wave has less dispersion, i.e., ω is more nearly $\propto k$ over a wide range of k than the compressional wave. The wave's propagation direction Θ is measured with respect to the primitive vector of the lattice. Reproduced from Fig. 3 of Ref. [12].

This lattice is characterized by two dimensionless parameters: the screening parameter $\kappa=a/\lambda_D$, which is typically ≈ 1 [8], and the Coulomb coupling parameter $\Gamma = Q^2/4\pi\epsilon_0 akT$, where T is the kinetic temperature of the particles (which may differ considerably from that of the plasma electrons and ions [4]). When $\Gamma \gg 1$, as in our experiments, the lattice is referred to as strongly coupled.

The elastic properties of an isotropic 2D lattice are completely defined by two independent elastic constants. There are several pairs of parameters that one may choose for this purpose, as for the case of an isotropic 3D body. For example, the two Lamé's coefficients may be used for this purpose [9].

The wake in a solid is more complex than that in a fluid because solids can support several different types of waves. A 2D crystalline lattice can vibrate in its plane with two kinds of sound waves, compressional and shear (i.e., transverse). In the compressional wave, the particles are displaced from their equilibrium positions in a direction parallel to the wave vector **k**. In the shear wave, the particles' displacement is perpendicular to **k**.

The dispersion relations of both compressional and shear waves in dusty plasmas have been derived theoretically in Refs. [10–17] and verified experimentally in Refs. [18–21]. Shown in Fig. 3 is the theoretical dispersion relation for a 2D triangular Yukawa lattice reproduced from Ref. [12]. The frequency is normalized by a 2D analog of plasma frequency

$\omega_0 = Q/(4\pi\epsilon_0 m a^3)^{1/2}$, where m is the particle mass. The compressional and shear modes both have an acoustic limit at long wavelengths, where $\omega \propto k$, as can be seen in the lower-left corner of Fig. 3, where the dispersion relations are straight lines. In this acoustic limit, the transverse wave sound speed C_T is about five times lower than the compressional wave sound speed C_L for typical experimental parameters. For shorter wavelengths, both kinds of waves exhibit dispersion, so that ω is not proportional to k. Compressional waves have much more dispersion than the shear waves, beyond the acoustic limit. The values of $ka = 0.6$ and 1.5 mark the onset of compressional wave's dispersion and its dependence on the lattice orientation, respectively, as shown in Fig. 3. The lattice orientation is measured as the angle Θ between the wave's propagation direction and the primitive vector of the lattice. Unlike compressional waves, shear waves are unable to propagate in an ordinary liquid or gas. Shear waves can propagate in a strongly coupled liquid only if the wavelength is comparable to the interparticle spacing a [14,17,22], in which case they are heavily damped by collisional viscosity.

The dispersion relation of compressional waves in a dusty plasma has a combination of both acoustic and dispersive characteristics. Correspondingly, a wake composed of these waves will have a structure containing both a Mach cone and multiple lateral and transverse wakes. This dual nature of the wake structure will be demonstrated in this paper using results from experiment, theory, and simulation.

Mach cones in dusty plasmas were theoretically predicted by Havnes *et al.* [23,24]. In a 3D dusty plasma, wakes composed of compressional waves might be excited by a moving boulder in Saturn's rings, as studied by Brattli *et al.* [25] using a fluid simulation. In a 2D lattice, Mach cones have been observed experimentally using two methods of excitation: by the Coulomb force from charged particles moving spontaneously beneath a 2D lattice [26,27], and by the radiation force from a spot of focused laser light swept across the lattice [28,29]. Wakes composed of compressional waves [25–28] have a structure resembling multiple nested cones, whereas wakes composed of shear waves have a single-cone structure, as predicted by Ma and Bhattacharjee [30] and observed experimentally in Ref. [29].

Mach cones have a larger opening angle for compressional waves than for shear waves. This distinction arises from the different sound speeds, $C_L \gg C_T$. With its slower sound speed, the shear wave generates a Mach cone with a smaller opening angle, according to Eq. (1).

Recently Dubin presented a theory [12] explaining the phonon wake structure behind a charge moving relative to a 2D plasma crystal. This theory explained the experimental results of Ref. [26], and predicted additional types of wakes, which we will investigate here.

In this paper, we report an experiment intended to observe and measure supersonic and subsonic wakes created in a 2D plasma crystal by a moving spot of laser light, and to verify the theoretical predictions of Ref. [12]. Experimental results of this paper were obtained in the same experiment reported in our previous paper, Ref. [29]. Here, we present additional experimental and simulation results; our analysis now includes calculation of the wake's full wave field using the theory of Ref. [12]. A method of calculating an experimental dispersion relation for a wave is developed, using only a snapshot of the wakes.

II. THEORY OF PHONON WAKES IN A 2D PLASMA CRYSTAL

To explain the phonon wake structure, the theory of Ref. [12] considers waves, both compressional and shear, with various wave numbers and directions of propagation, which are excited by a moving disturbance. Waves with a certain wave number k propagate with a phase speed $C(k) \equiv \omega/k$, where the wave frequency $\omega(k)$ is determined by the wave's dispersion relation. In the acoustic limit $C(k) = C$, but at shorter wavelengths, $C(k)$ depends on k. Because the medium is dispersive, Eq. (1) must be modified so that it expresses a Mach condition for only one value of k at a time: $C(k) = U\sin[\Theta(k)]$, which means that waves with different wave numbers k propagate at different angles $\Theta(k)$. Phase mixing of the various excited waves gives rise to constructive and destructive interference. The resulting interference pattern determines the appearance of the phonon wake. The waves are assumed to be linear in this theory.

The theory of Ref. [12] predicts that the phonon wake structure in a 2D plasma crystal depends on the speed of the moving disturbance U and the crystal's screening parameter κ. For $U > C$ the resulting wake consists of a Mach cone, a multiple-cone lateral wake, and a narrow wake formed by umklapp phonons (phonons from beyond the first Brillouin zone of the lattice). For $U < C$ the Mach cone disappears and is replaced by a transverse wake. The effect of κ is to change the scale length of the wake. For a fixed $U > C$, the scale length increases roughly as $\kappa^{-2/3}$ for $\kappa^{-1} > 1$.

III. EXPERIMENTAL METHOD

We used the experimental setup of Fig. 2(b), which was described previously in Ref. [29]. A plasma was produced using a capacitively coupled rf discharge. We used 20 W of rf power at 13.56 MHz, with an amplitude of 84 V peak to peak. The self-bias voltage was -61 V. To reduce the damping rate, we used Ar at a pressure of only 15 mTorr, corresponding to a gas drag, which is accurately modeled [31] by the Epstein expression, of $\nu = 2.9\ \mathrm{s}^{-1}$.

A monolayer of polymer microspheres was suspended in the plasma sheath above the discharge's lower electrode, and they arranged themselves in a triangular lattice with hexagonal symmetry. The particles acquired a high negative charge by collecting electrons and fewer ions. In the vertical direction, the particles were levitated by a balance between the Coulomb force and gravity.

In the horizontal direction, they repelled each other but were confined by the plasma's natural ambipolar electrostatic fields. Our lower electrode is flat out to a radius of 10.7 cm, where there is an elevated lip at the electrode's perimeter. The particle suspension, however, had a much smaller radius of 2.5 cm, so that the radial fields were not due to the lip. These radial fields arise naturally due to gradients in the

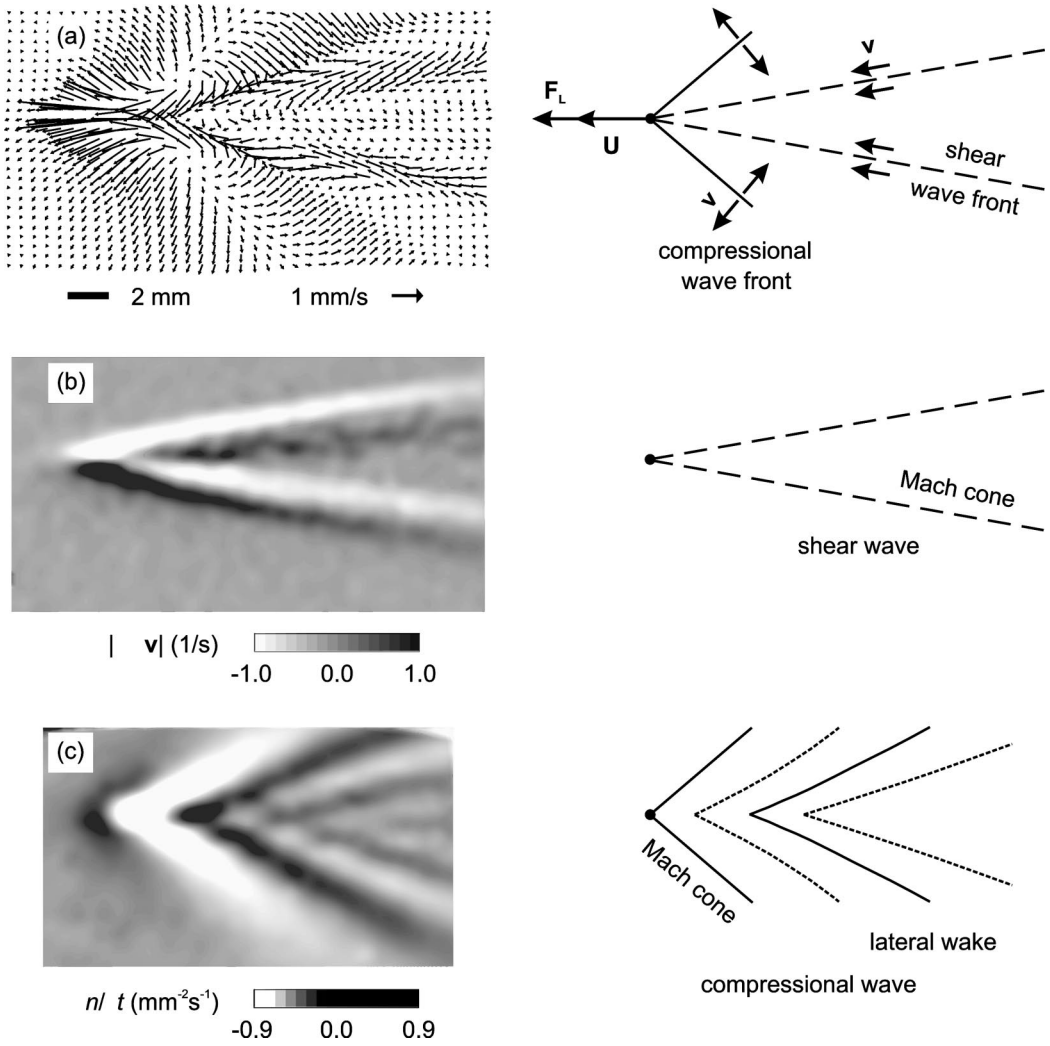

FIG. 4. The compressional- and shear-wave Mach cones, excited simultaneously. The scanning speed U is higher than the sound speed for both the compressional and shear waves. Maps are shown for (a) particle velocity $\mathbf{v}$, (b) vorticity $|\nabla\times\mathbf{v}|$, and (c) $\partial n/\partial t$, where n is the particle areal number density.

number density and ionization rates, in the glow discharge. Our experimental conditions were similar to those of Ref. [31] (though an additional confining ring was used in Ref. [31]), where the confining potential was measured to have a parabolic shape.

The microspheres had a diameter of 8.09 ± 0.18 μm as measured using TEM, and a mass density of 1.51 g/cm^3. The lattice had a diameter of about 50 mm, and an interparticle spacing of $a=762$ μm, which varied by ±46 μm within our viewing region.

The Coulomb coupling parameter Γ of the lattice was calculated to be $\Gamma\approx11\,500$ and $\Gamma\exp(-\kappa)\approx2700$. The crystal's kinetic temperature $T=380$ K was calculated by fitting the particle velocity distribution of the undisturbed crystal to a Maxwellian distribution. The particle charge was measured to be $Q=-14\,100e$, as we will describe in Sec. IV C. Our lattice had rather high value of Γ, which is consistent with its crystalline state [32]. As another indication of the ordered state of the lattice, we note that the pair correlation function $g(r)$ had many peaks, and the translational order length was from $4a$ to $18a$.

The particles were viewed through the top window by a video camera. They were illuminated by a horizontal He-Ne laser sheet. The camera's field of view was 24×18 mm, and it included about 850 particles. The images were digitized with an 8-bit gray scale and a 640×480 pixel resolution. Particle coordinates and velocities were then calculated using a method providing subpixel spatial resolution [28], and the velocity field was then mapped onto a fixed grid.

In our experiment, we sought to observe the phonon wake's features in the region along the wake's symmetry axis, corresponding to smaller opening angles. These features were predicted by Dubin in Ref. [12]. In the earlier experiment of Ref. [28] this region was highly perturbed, obscuring any small-angle features that might be present. To avoid perturbing this region we used two variations of the laser-excitation technique of Melzer *et al.* [28]. For our main experimental results, the laser spot was moved in the direction perpendicular to the laser beam, i.e., perpendicular to the momentum imparted to particles by the laser radiation force $\mathbf{F}_L$. In this approach, the region corresponding to smaller opening angles was not perturbed. We also report some re-

sults using, as an alternative method, a laser spot that was moved in the direction of the laser beam. The latter method is similar to that of Ref. [28] except that we used a reduced laser power so that the region behind the moving spot was not perturbed much. At its focus in the vacuum chamber, the Ar^+ laser beam had a power of 0.6 W, which we reduced to as little as 0.12 W for our slowest scanning speeds, to avoid melting the lattice.

We recorded a digital movie, consisting of ten frames at 30 frames/s, as the laser spot was scanned across the lattice. The video was synchronized to the motion of the laser beam using the triggering scheme of Ref. [28]. This allowed us to average the data from over 100 scans, under the same conditions, to improve the signal-to-noise ratio. The scans were repeated at an interval of 5.9 s, allowing the crystal to have sufficient time to relax after the disturbance created by the previous scan.

We verified, by using a side-view video camera, that there was no out-of-plane buckling of our 2D lattice. The particle motion was thus restricted to be in the horizontal plane and our plasma crystal was truly 2D.

IV. EXPERIMENTAL AND THEORETICAL RESULTS

A. Review of previous results

In Ref. [29], we reported a measurement of sound speeds, for the same experiment where we obtained the results presented below. Pulses of compressional and shear waves were launched in the lattice to measure the sound speeds using the methods of Refs. [33,21]. The pulses were excited by stimulating the particles with an Ar^+ laser sheet that was chopped on and off. The sound speeds of the two modes were measured to be $C_L = 24.2 \pm 1.7$ mm/s and $C_T = 5.4 \pm 0.5$ mm/s, for the compressional and shear waves, respectively.

The ratio of the two sound speeds, $C_L/C_T = 4.48 \pm 0.52$, is expected for our experimental conditions. This value corresponds to $\kappa = 1.19 \pm 0.28$, according to the theory of waves in a Yukawa crystal [13,20]. The particle charge is then calculated to be $Q = -12\,700 \pm 1200e$ using the method of Ref. [20] based on the theory of Ref. [13]. As an independent test, we also used a variant of the resonance method of measuring particle charge [34], which gave a lower value of $Q = -8800e$. We believe this resonance method is less precise than methods relying on the wave dispersion relation, for a purely 2D lattice with an interparticle potential that is nearly Yukawa, like ours.

In Ref. [29], we excited both compressional- and shear-wave Mach cones simultaneously when we swept the laser spot in the direction of the laser beam, as in Ref. [28], at a reduced laser power so that the region behind the moving spot was not perturbed by defect generation (Fig. 4). The laser beam, which had a power of 0.24 W, was swept through the lattice with a speed higher than both the compressional- and shear-wave sound speeds. When we increased the excitation laser power to 0.6 W and the rf power to 30 W, the shear Mach cone disappeared, replaced by a disordered region behind the moving spot, as in Ref. [28].

Experimentally, compressional waves can be distinguished from shear waves using three kinds of maps. First, in a map of particle velocity **v**, the two modes differ in the direction of the particle motion as compared to the direction of the wave propagation. These directions are parallel in the compressional wave and they are perpendicular in the shear

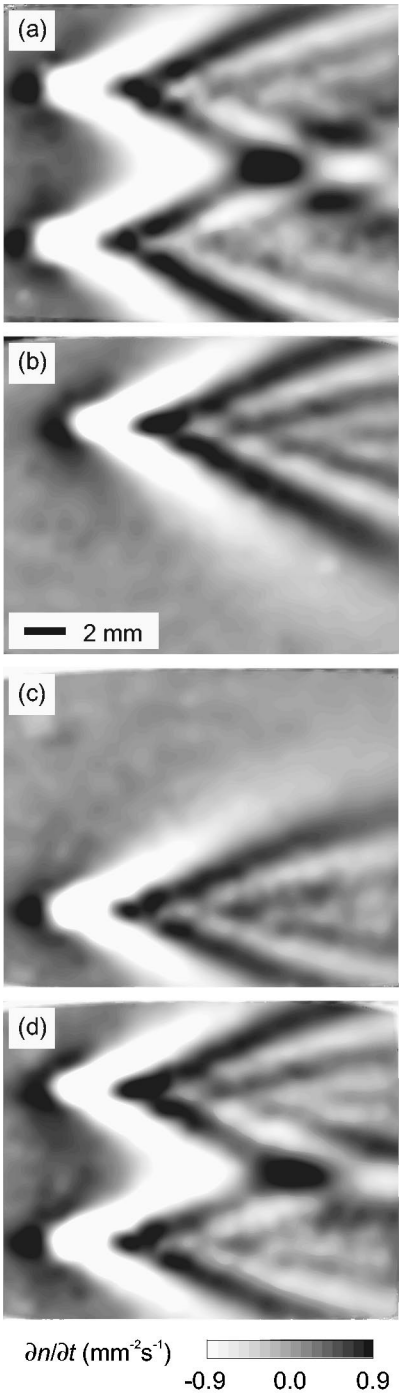

FIG. 5. The test of the phonon wake linearity. Maps are shown for $\partial n/\partial t$, where n is the particle number density, to reveal the compressional waves. Experimentally observed were (a) the double wake and (b),(c) two separate single wakes. The double-wake structure in (d) was synthesized as a linear superposition of (b) and (c). The linear superposition in (d) is similar to the experimental wake in (a), which means that the experimental wake is linear, in its far field.

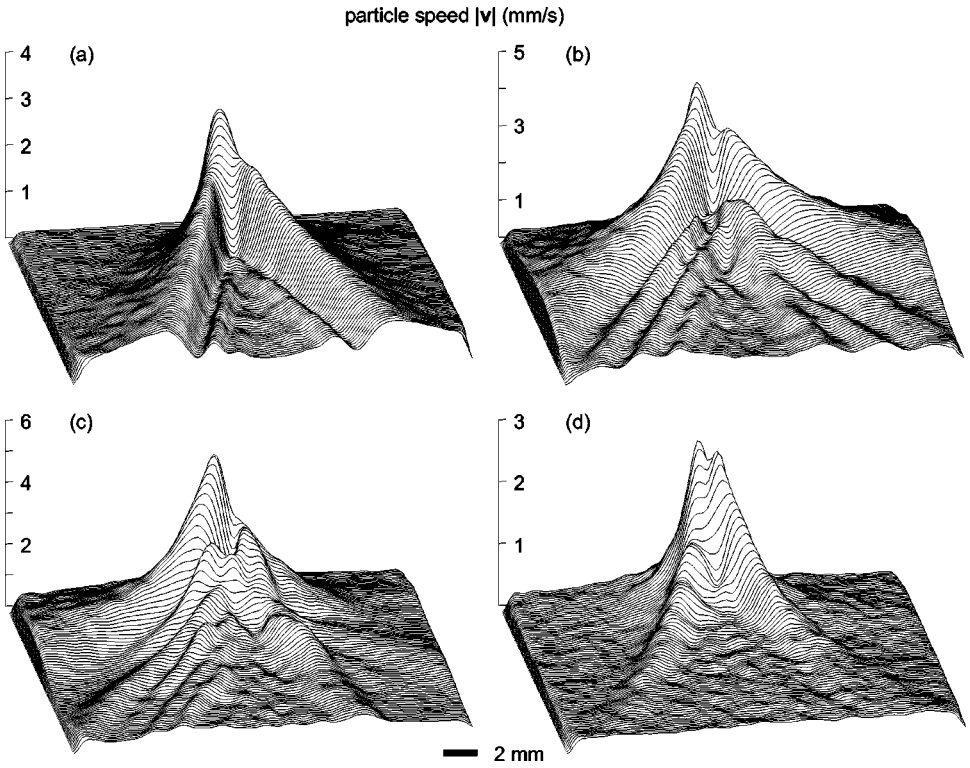

FIG. 6. Four different types of phonon wakes depending on the speed of scanning U as compared to the compressional wave's sound speed C_L: (a) $U/C_L = 2.14$, (b) $U/C_L = 1.17$, (c) $U/C_L = 0.87$, (d) $U/C_L = 0.49$. We refer to the latter two as "subsonic," although they are supersonic with respect to the shear wave. Maps are shown for the particle speed v.

wave. For example, we can clearly distinguish the compressional-wave Mach cone with its bigger opening angle and the shear-wave Mach cone with its smaller opening angle in Fig. 4(a), based on the direction of the particle motion in the cones' wings.

Second, compressional waves appear in a map of $\partial n/\partial t$, where n is the particle areal number density. In the linear approximation, $\partial n/\partial t = -n(\nabla \cdot \mathbf{v})$. The $\partial n/\partial t$ map in Fig. 4(c) shows a compressional-wave Mach cone. This type of map, also called a numerical Schlieren map [28], is effective for detecting compressive particle motion.

Third, shear waves appear in a map of the vorticity $|\nabla \times \mathbf{v}|$. The $|\nabla \times \mathbf{v}|$ map in Fig. 4(b) shows the shear-wave Mach cone. The vorticity of the Mach cone demonstrates that the motion has significant shear. (Unlike a fluid, however, our medium is elastic, and it oscillates without breaking bonds after it is perturbed. Thus, although the particle motion has a momentary vorticity, there is no vortex with particle circulation.) In analyzing our experimental images of the phonon wakes, we will use the $|\nabla \times \mathbf{v}|$ maps to reveal the shear waves, and $\partial n/\partial t$ or $\nabla \cdot \mathbf{v}$ maps to reveal the compressional waves.

B. Test of linear superposition

We performed a test to verify that linear superposition occurs. Such a test is valuable to verify whether the theory of Ref. [12], which relies on linear superposition, is valid. To do this, we excited two identical wakes simultaneously by sweeping two laser spots in parallel through the lattice. Each wake consisted of the compressional- and shear-wave Mach cones, and multiple-cone compressional wake. The compressional component of the double-wake is shown in Fig. 5(a). In two separate experiments, an individual wake was excited, by blocking one or the other laser beam, as shown in Figs. 5(b) and 5(c). A double-wake structure was then artificially synthesized by adding up the maps of the two individual wakes, as shown in Fig. 5(d). The experimental and synthesized double-wake structures are similar, which means that linear superposition is occurring in Fig. 5(a).

This test proves linearity only in the far field, i.e., not near the excitation spot. In the near field the linearity might break, as the particle speed v reaches relatively high values with v/C_L in the range of 0.12–0.23, depending on the scanning speed. Previously, nonlinear effects were found to be significant for the compressional waves in a 2D plasma crystal for the wave amplitudes $v > 0.07 C_L$ [33]. Nonlinearity in the near field can, however, affect the wake structure in the linear far field, as we will demonstrate in Sec. V using a MD simulation.

The linearity of the wakes implies that Dubin's theory of wakes in a 2D plasma crystal [12] is applicable in the far field. We compare our experimental results to this theory. We performed the above test of linearity only for a single value of the scanning speed, corresponding to a compressional Mach number U/C_L of 1.38. Nevertheless, as we will see below, the experimentally observed wakes agree with the theory [12], which is essentially linear, in the entire range of the scanning speeds that we used.

C. Wake results from experiment and theory

We observed several distinct types of phonon wakes behind the moving laser spot, depending on its speed, which was varied from supersonic to subsonic with respect to the sound speed of the compressional waves. The wake structure was mostly just a single cone when the compressional Mach number $M = U/C_L$ was $\gg 1$ and $\ll 1$, as in Figs. 6(a) and

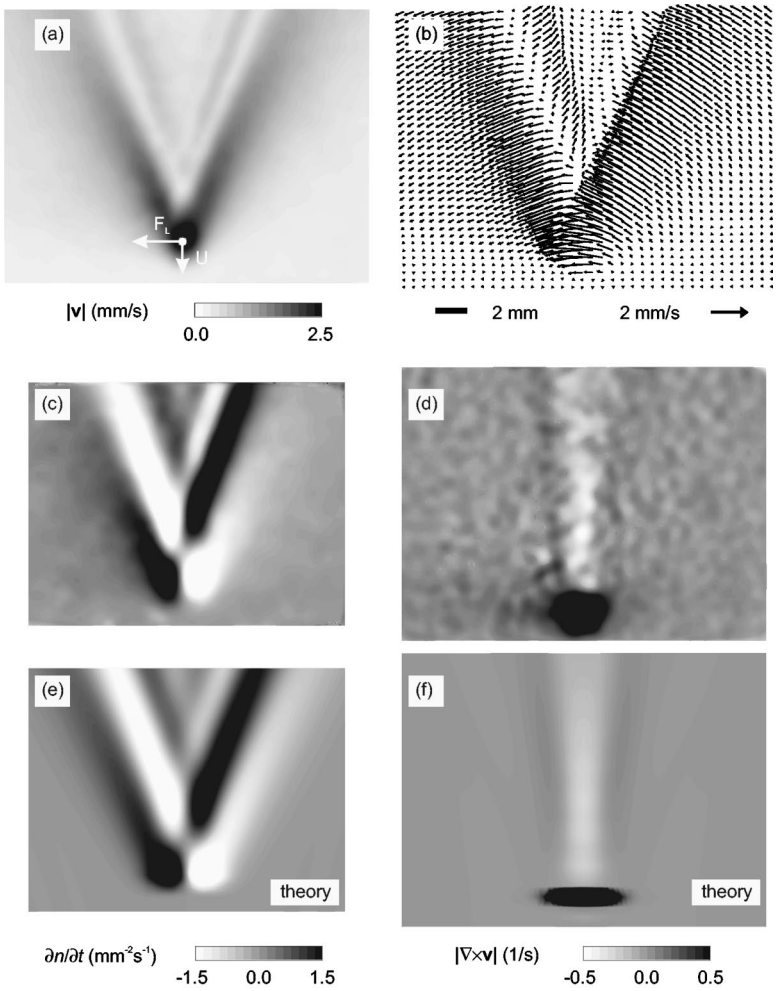

FIG. 7. A compressional-wave Mach cone at the speed of scanning $U/C_L = 2.14$. Maps are shown for (a) particle speed v, (b) vectors of particle velocity $\mathbf{v}$, (c) experimental and (e) theoretical values of $\partial n/\partial t$, where n is the particle number density, (d) experimental and (f) theoretical values of vorticity $|\nabla \times \mathbf{v}|$.

6(d), respectively. The wakes had a more complicated multiple-cone structure when $M \approx 1$, as in Figs. 6(b) and 6(c), for slightly supersonic and subsonic conditions, respectively. Below we will analyze the structure of these wakes.

First we examine a strongly supersonic wake at $U = 2.14C_L$ in Fig. 7. The wake's structure, as shown in the velocity maps of Figs. 7(a) and 7(b), contains both compressional and shear wakes, but the latter are much less prominent at such a high Mach number. Comparing the $\partial n/\partial t$ map of Fig. 7(c), which shows the compressional wake to the $|\nabla \times \mathbf{v}|$ map of Fig. 7(d), showing the shear wake, we see that most of the particle motion in the far field is attributable to compressional waves. Shear motion is present only within the near-field region of the laser spot and in a very narrow angle behind the spot. This small angle is as expected, because for these conditions $U/C_T = 8.6$ so that Eq. (1) predicts $\mu \approx 7°$ for the shear waves. The compressional wake has a multiple-cone structure; we identify the first cone as the Mach cone and the second cone, at a smaller angle, as a lateral wake. We also show theoretical results in Figs. 7(e) and 7(f), computed using Dubin's theory of Ref. [12] with the same parameters as in the experiment. These include parameters describing both the dusty plasma (i.e., particle charge Q, interparticle spacing a, and screening length λ_D) and the laser beam, which is assumed to have a Gaussian profile with a full width at half maximum of 0.36 mm.

Reducing the speed U to a barely supersonic $1.17C_L$ in Fig. 8, we again see a multiple compressional wake, and at this lower speed we can also more easily identify a shear-wave Mach cone. The latter is visible in the $|\nabla \times \mathbf{v}|$ map of Fig. 8(d). The compressional wake's structure is generally similar to that at the higher Mach number except that we can identify a larger number of lateral wakes and, as expected, the opening angle of the Mach cone is larger. For both waves, the wake structures observed in the experiment and predicted by theory in Figs. 8(e) and 8(f) show a close resemblance.

The multiple-cone structure of compressional wakes arises from the wave dispersion. The compressional wake structure consists of a Mach cone followed by a series of lateral wakes. Previously, Melzer *et al.* [28] identified the lateral wakes as additional Mach cones, but we now recognize that they are lateral wakes, similar to ship's wakes, arising from the wave's dispersion as predicted by Dubin's theory of Ref. [12]. Depending on the conditions, in our experiment we observed various numbers of lateral wakes. There are three such wakes in Fig. 8(a) at $U = 1.17C_L$, and five at $U = 1.07C_L$.

The single Mach cone structure of shear wakes is due to the nearly dispersionless character of shear waves. While this wave does have dispersion for large wave numbers, it is not

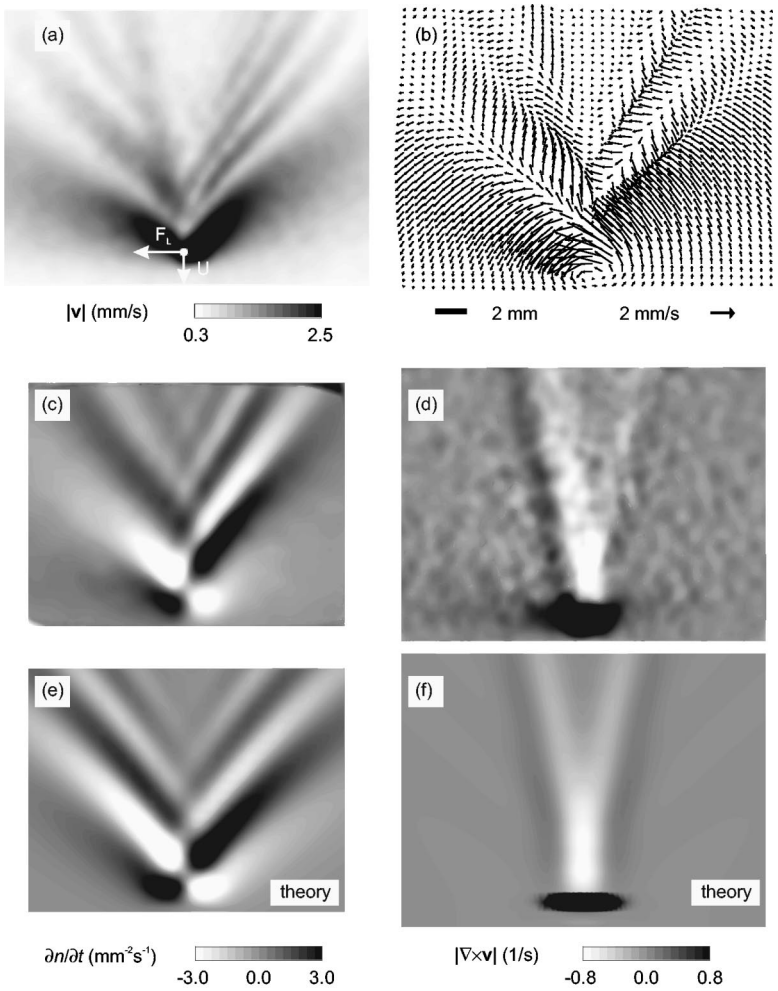

FIG. 8. Compressional- and shear-wave Mach cones and supersonic lateral wakes at the speed of scanning $U/C_L=1.17$. Maps are shown for (a) particle speed v, (b) vectors of particle velocity $\mathbf{v}$, (c) experimental and (e) theoretical values of $\partial n/\partial t$, where n is the particle number density, (d) experimental and (f) theoretical values of vorticity $|\nabla\times\mathbf{v}|$.

revealed in our wake. Apparently in our method only smaller wave numbers are excited with enough efficiency to be observed.

Reducing the speed further to $U=0.87C_L$, which is barely subsonic for compressional waves and supersonic for shear waves, we see a structure in Fig. 9 with most of the features of the supersonic wake at $U=1.17C_L$ in Fig. 8. What is most prominent in the compressional wake structure at a slightly subsonic speed is the lateral wake. One would expect the Mach cone for compressional waves to disappear as U/C_L is reduced below unity, although this is not easily seen in the maps. The leading cone of the lateral wake might be confused with a Mach cone, but because of the independently measured sound speed we know that $U/C_L<1$ so that Eq. (1) does not predict a measurable Mach cone angle. The shear waves for this scanning speed again formed only a Mach cone, shown in Fig. 9(d).

The observed wake structure agrees with that predicted by the theory of Ref. [12], shown in Figs. 9(e) and 9(f). There is however a discrepancy. The theory of Ref. [12] predicts outward bending of the lateral wake's wings, as shown in Fig. 9(e). However, in our experiment they bend outwards and then inwards at a longer distance from the exciter, as shown in Fig. 9(c). The same discrepancy, albeit less prominent, was also observed for the supersonic wake at $U=1.17C_L$ in Fig. 8. We will explain this discrepancy in Sec. V using a MD simulation.

Reducing the speed down to $U=0.49C_L$, which is very subsonic for compressional waves but still supersonic for shear waves, we see a quite different structure, shown in Fig. 10, with a different type of compressional wake, the transverse wake, and a distinctive Mach cone made of shear waves. The compressional waves no longer formed a multiple-cone structure. They produced neither a Mach cone nor a strong lateral wake. Instead, they formed a set of stripes, perpendicular to the direction of scanning, similar to the transverse wake behind a ship moving in deep water shown in Fig. 1. This subsonic transverse wake was predicted by the theory of Ref. [12], as shown in Fig. 10(e). It had a relatively short wavelength $\lambda=2a$. The effective excitation of short-wavelength compressional waves in our experiment is explained by the relatively small size of the excitation laser spot in the direction of scanning, which was comparable to the interparticle distance a. We observed a smooth transition from a strong lateral wake to a strong transverse wake, as we varied the scanning speed from $U/C_L=0.97$ downward to 0.49.

The Mach cone angle relation $\sin\mu=C/U$ is shown in Fig. 11 to be obeyed for both the shear- and compressional-wave

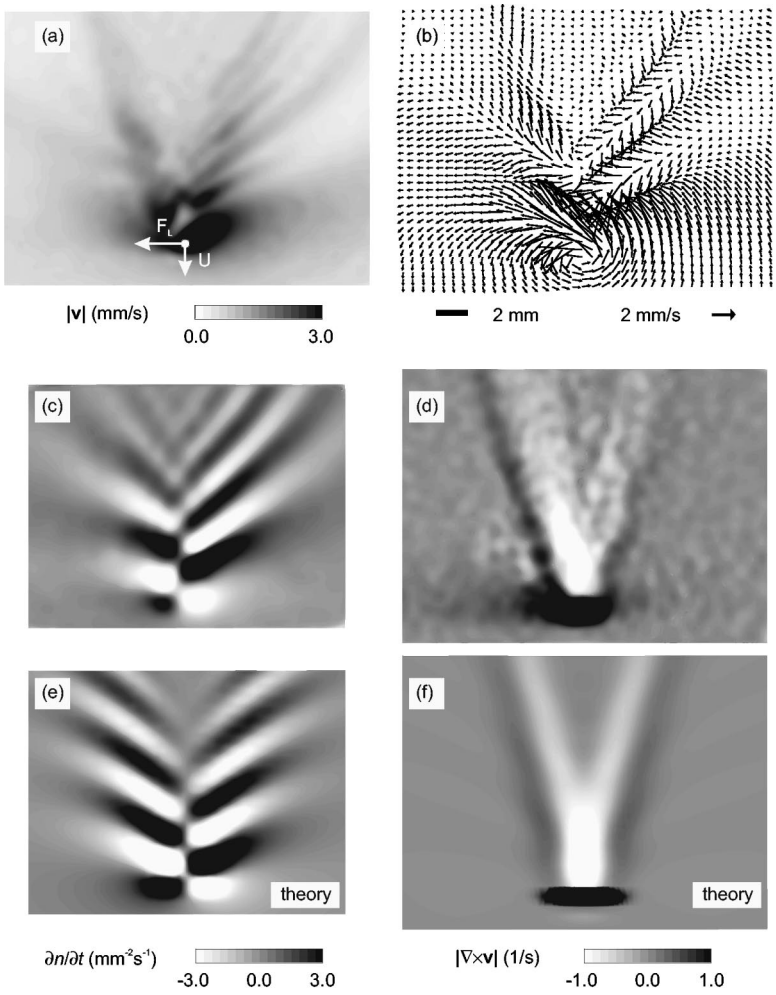

FIG. 9. Subsonic lateral wakes and a shear-wave Mach cone at the speed of scanning $U/C_L = 0.87$. Maps are shown for (a) particle speed v, (b) vectors of particle velocity $\mathbf{v}$, (c) experimental and (e) theoretical values of $\partial n/\partial t$, where n is the particle number density, (d) experimental and (f) theoretical values of vorticity $|\nabla \times \mathbf{v}|$.

Mach cones, over a wide range of scanning speeds. The angle μ was measured from speed maps, like those in Figs. 7(a), 8(a), 9(a), and 10(a). The slope in Fig. 11 gives $C_T = 5.7 \pm 0.4$ mm/s and $C_L = 23.0 \pm 1.0$ mm/s. These values are consistent with the preliminary measurements using compressional- and shear-wave pulse propagation. The sound speed measurements made from the Mach cones are based on more experimental data. The values of the screening parameter and the particle charge, calculated using the method of Ref. [20] based on the theory of Ref. [13] using the sound speeds from the Mach cone angles, are $\kappa = 1.45 \pm 0.24$ and $Q = -14\,100 \pm 1000e$, respectively.

V. DETERMINING THE DISPERSION RELATION FROM A 2D WAKE STRUCTURE

Below we will present a generally useful method of determining the dispersion relation from an experimental measurement of the wake. This method is applicable to a local disturbance in a monolayer or to a 3D wake if it has a 2D symmetry. This method relies on maps of the wakes, and it assumes nothing about the interparticle potential. It does assume that the wake's structure is determined by the wave's dispersion. We developed this method so that it yields a dispersion relation, calculated from the experimental data. For the plasma crystal, the resulting experimental dispersion relation is shown to be useful for calculating the values of κ and Q.

A. General method

Because the wake structure in the far-field results from the interference of waves of different wave numbers, and these wave numbers all obey the dispersion relation, it is possible to determine the dispersion relation from the wake structure, as we shall do here. This is the opposite of the process described in Ref. [12], where the dispersion relation is used to predict the wake structure. It is possible to adopt either approach because the far-field wake contains linear waves whose structure is determined by a combination of the dispersion relation and the conditions in the near field where the waves are excited.

Our approach, sketched in Fig. 12, relies on measuring the angle of the wave fronts of the lateral wake. We start with an experimental map of the particle speed like Fig. 8(a), or some other parameter such as $\partial n/\partial t$. Next, we manually draw contours of the wave fronts, i.e., the crests and troughs of the lateral wake pattern. We also draw a pair of straight lines to identify the Mach cone, if one exists, and its apex. Thus we obtain a diagram like Fig. 12(a). In this diagram, we then measure various angles and distances, as explained below.

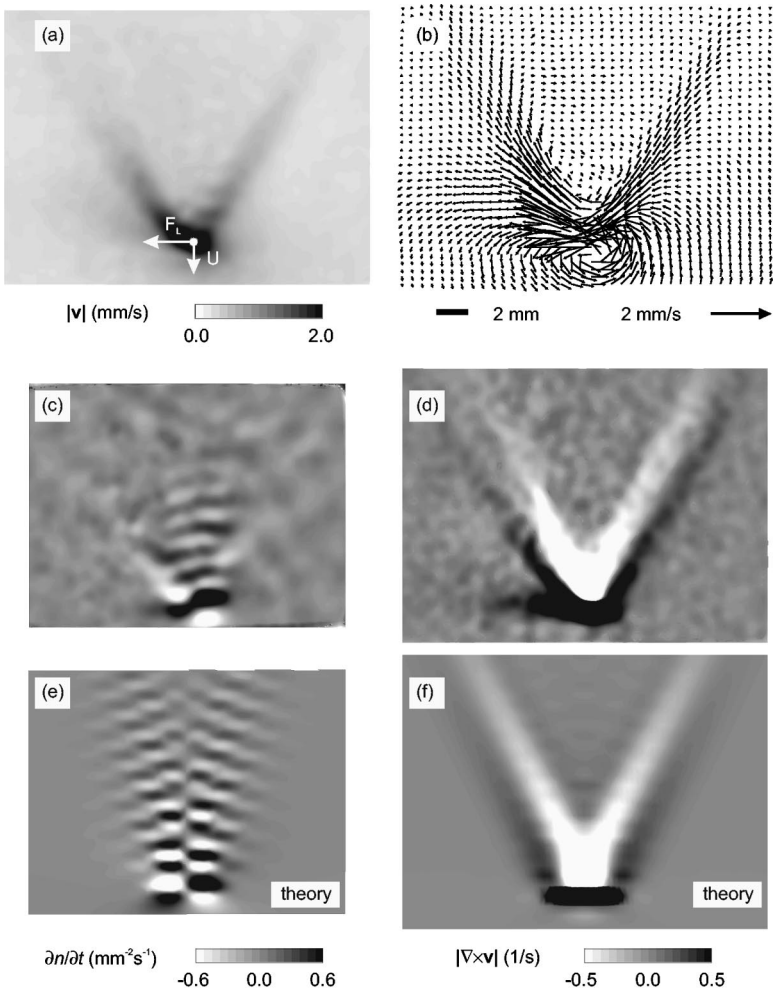

FIG. 10. Subsonic transverse wakes and a shear-wave Mach cone at the speed of scanning $U/C_L = 0.49$. Maps are shown for (a) particle speed v, (b) vectors of particle velocity $\mathbf{v}$, (c) experimental and (e) theoretical values of $\partial n/\partial t$, where n is the particle number density, (d) experimental and (f) theoretical values of vorticity $|\nabla \times \mathbf{v}|$.

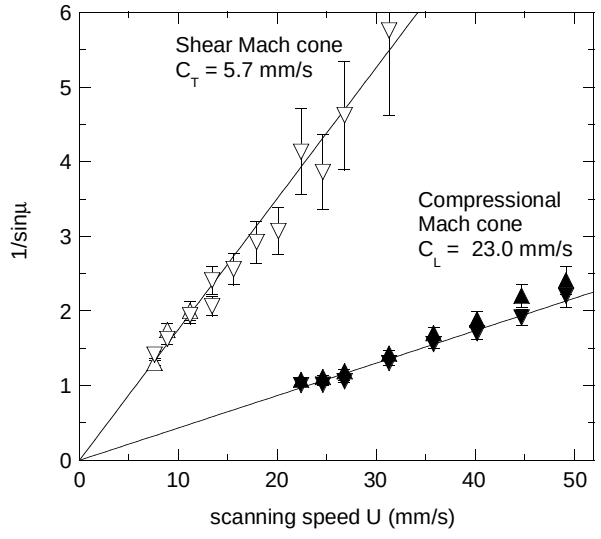

FIG. 11. Test of the Mach cone angle relation $\sin \mu = C/U$, where μ is the cone's opening angle, U is the speed of the supersonic disturbance, and C is the sound speed, for shear and compressional Mach cones. Here, μ is measured separately ($\triangle$) at the laser-excitation side and ($\triangledown$) at the opposite side of the particle-speed maps like those in Figs. 7(a), 8(a), 9(a), and 10(a).

Our analysis of the angles relies on the theory of Ref. [12] for the lateral wake. A spectrum of waves is launched by the moving disturbance. There is a superposition of waves that originated at different times, when the moving disturbance was located at correspondingly different positions. These waves all interfere with one another, yielding the wake structure. As a result of all this, there are two properties of the lateral wake structure that we can relate to the dispersion relation. Referring to Fig. 12, we now explain them.

First, all points along any chord, at angle β from the apex, correspond to wave energy composed solely of a single wave number k, as shown in Fig. 12(b). The chord represents the locus of the radii of all the circular wave fronts for a particular value of k, as sketched in Fig. 2(a). In other words, the geometry dictates a one-to-one relationship between any angle β that one chooses and k. From the experimental maps, we measure the wavelength $\lambda = 2\pi/k$ as the distance between the crests or troughs.

Second, the waves at each value of k will satisfy their own Mach condition, with a phase velocity $C(k) \equiv \omega/k = U \sin \Theta(k)$. Here, the angle Θ is measured as the normal to the wave front, as shown in Fig. 12(c).

Combining these two relationships, and using them with an experimental map of the wake structure, we can determine the dispersion relation as a graph of wave number vs frequency. This is done from a single map from the experiment.

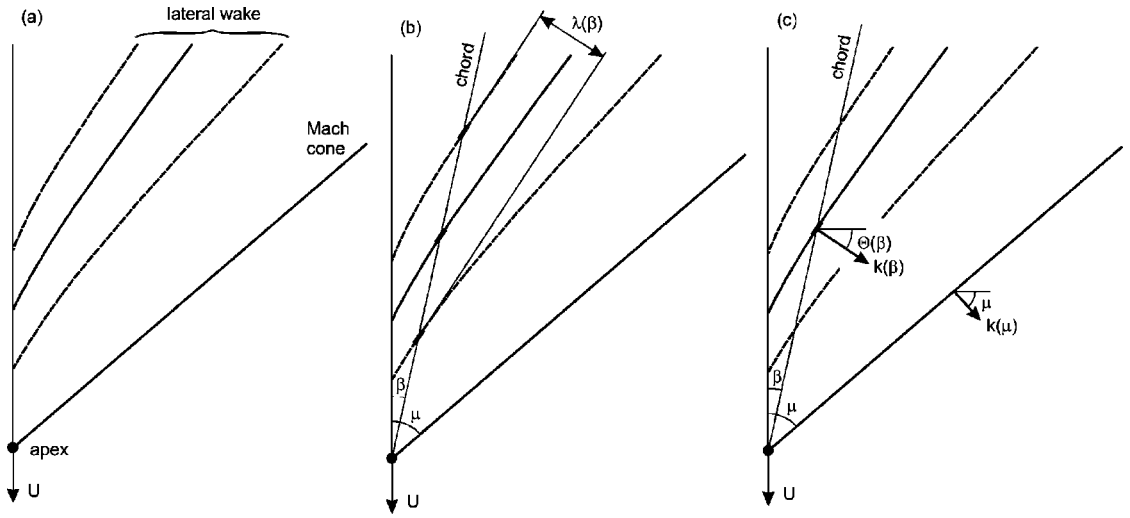

FIG. 12. Spatial structure of a supersonic compressional phonon wake according to the theory of Ref. [12]. (a) A lateral wake and a Mach cone are excited by a moving disturbance. (b) All points along any chord, at angle β from the apex, correspond to a single wave number $k=2\pi/\lambda$, where λ is the wavelength. (c) The waves at each value of k satisfy their own Mach condition, $\omega/k=U\sin\Theta(k)$. Our method of determining a wave's dispersion relation from the wake pattern relies on this three-step construction. Each value of β yields a single point on the dispersion relation. Shown in this figure is one-half of the wake at the speed of scanning $U/C_L=1.17$.

We draw lines on the wave fronts of the lateral wakes and Mach cones, measure their angles Θ and wavelengths λ along chords at various angles β, and then compute k from λ, and ω from Θ and k. In each instance this measurement yields a data point for the dispersion relation on the ω-k plane. Repeating for various angles β, we measure the dispersion relation ω vs k. Here, k denotes the real part of the wave number.

It is possible also to measure the imaginary part of k by quantifying the amplitudes of the waves and measuring their damping. This is analogous to using the amplitude vs distance relationship of an externally excited sinusoidal wave to obtain the imaginary part of k. In the demonstration presented in Sec. V B, we do not attempt this, however.

This method of measuring the dispersion relation has the advantage that it requires only a single snapshot of the wake. Other methods of measuring a dispersion relation typically require a series of measurements that must be made at different times. For example, one method is to excite the sample with a sinusoidal disturbance and then to measure the phase and amplitude of the wave, propagating away from its source. This requires a series of measurements for at least one full period of the wave [18,20,31]. Another method is to measure a series of velocity or density maps, with or without any external excitation, and compute the power spectrum in ω and k space [35]. Unlike these methods, which all require a series of data recorded over time, the method we presented here uses only the spatial structure from a single snapshot (it also requires knowledge of the speed U of the moving disturbance). As a practical matter, however, to attain a satisfactory signal-to-noise ratio in a map of the wake, it may be necessary to average many maps.

B. Application of the method to a plasma crystal

We used the method described above to calculate the dispersion relation in our 2D plasma crystal. The result is shown in Fig. 13. We found that it was possible to use either maps of particle speed or $\partial n/\partial t$. For the subsonic case of $U/C_L=0.49$, we found that the $\partial n/\partial t$ map was required, and in this case we obtained only a single point, for ω vs k, using the transverse wake. For the supersonic cases of $U/C_L=1.17$ and 1.35, we used speed maps of the lateral wakes. While it is in general possible to measure the dispersion relation from a single map of the wake, we found that we could

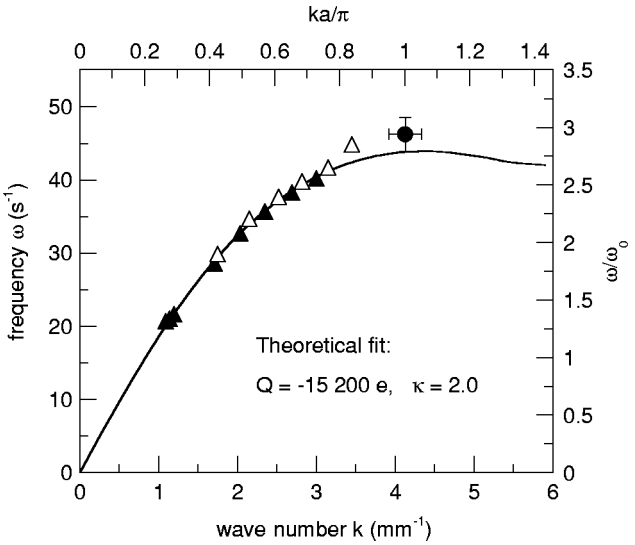

FIG. 13. Experimentally measured dispersion relation of compressional waves. The points were calculated using the theoretical construction [12] of the dispersion relation, as shown in Fig. 12, from the particle-speed maps of (▲) the lateral wake at the speed of scanning $U/C_L=1.17$ in Fig. 8(a) and (△) the lateral wake at $U/C_L=1.35$, and (●) the $\partial n/\partial t$ map of the transverse wake at $U/C_L=0.49$ in Fig. 10(c). The best fit using the theory of Ref. [12] gave the particle charge $Q=-15\,200e$ and screening parameter $\kappa=2.0$.

obtain more data, and extend the range of k, by repeating the measurement for three values of U. We note that these three measurements all yield data points lying on a common curve in Fig. 13.

The dispersion relation of compressional waves contains useful information about the interparticle potential. For a plasma crystal, this potential is characterized by the screening parameter κ and particle charge Q. In order to extract these parameters from our experimental data, we fitted the experimentally measured real part of the dispersion relation using a simple cubic approximation $\omega(k)=C_L k-Ak^3$ (Eq. (11) of Ref. [12]), in the range of $ka\leqslant 1.3$. The best values of the fitting parameters were $C_L=20.0$ mm/s and $A=1.12$ mm^3/s. Using these values, and Eqs. (A7) and (A9) of Ref. [12], we found $\kappa=1.77$ and $Q=-14\,100e$. The cubic approximation of $\omega(k)$ is only accurate for $ka<1$; therefore, the resulting values of κ and Q have a limited accuracy.

A method with a higher accuracy for extracting the values of κ and Q from the experimental dispersion relation is to fit the latter in the entire experimentally measured range of k to a theoretical curve. As there is no exact analytical expression for $\omega(k)$ in the wide range of k, it must be determined numerically for different values of κ and Q. The best fit of the experimental dispersion relation using the theory of Ref. [12], which assumes a triangular lattice with a Yukawa potential, is shown in Fig. 13. Theoretical values of $\omega(k)$ were averaged over all possible angles Θ between the wave vector $\mathbf{k}$ and the lattice primitive vector, to more nearly correspond to experimental conditions where we averaged 100 maps, over a period of time, as the plasma crystal slowly rotated. In the experiment this averaging was necessary to improve the signal-to-noise ratio by smoothing the structure in the map due to the particle discreteness, as well as reducing the significance of any momentary anomalous disturbances in the lattice. The fitting parameters were κ and Q, all other parameters were chosen as in the experiment. The best fit corresponds to the values of $\kappa=2.0$ and $Q=-15\,200e$. This method gave somewhat bigger values of κ and Q, as compared to the methods based on the measurement of the compressional- and shear-wave sound speeds using pulses (Sec. IV A) or Mach cones (Sec. IV C).

VI. MOLECULAR DYNAMICS SIMULATION

A. Simulation of the experiment

We performed a 2D MD simulation using parameters similar to those of the experiment, Figs. 7–10. The particle equation of motion $md^2\mathbf{r}/dt^2=-Q\nabla\phi-m\nu d\mathbf{r}/dt+\mathbf{F}_L$ was integrated for 5000 particles. The electric potential ϕ consisted of a harmonic potential for the external radial confinement $-m\Omega^2\rho^2/2$ plus a binary interparticle repulsion, assuming a Yukawa model. Here ρ is the distance from the central axis and Ω is the sloshing-mode frequency, corresponding to the confining potential. We used the parameters $Q=-14\,100e$, $\lambda_D=526$ μm, $m=4.2\times10^{-13}$ kg, and $\nu=2.9$ s^{-1} for Epstein drag. We chose $m\Omega^2=2.4\times10^{-13}$ kg/s^2 to obtain a lattice with a particle separation of 762 μm in the center; this corresponds to $\Omega=0.76$ s^{-1}. After the particles formed a crystal, we introduced a moving localized force $\mathbf{F}_L$ to model the force due to the moving laser spot. To simulate the shape of the laser spot, the force had an elliptical Gaussian profile, as in Ref. [29]: $\mathbf{F}_L=f_0\exp(-x^2/b_x^2)\exp[-(y-Ut)^2/b_y^2]\mathbf{x}$, with $b_y=0.26$ mm, $b_x=b_y/\sin10°=1.48$ mm, and $f_0=1.7\times10^{-13}$ N (reduced to 0.6×10^{-13} N for the slowest excitation with $U=11.2$ mm/s). We varied the laser spot speed in the range of $U=11.2$–49.2 mm/s.

For each value of the laser spot speed, we averaged 40 runs of the simulation each corresponding to a different angle Θ of motion of the laser spot with respect to the primitive vector of the lattice. The values of Θ were evenly spaced in the interval of 0°–360°. This averaging allowed us to improve the signal-to-noise ratio and to perform a more accurate modeling of our experiment, where 100 maps were averaged and Θ was continuously changing due to a slow self-rotation of the plasma crystal. Due to this averaging the results of our simulation, as well as our experimental data, are not Θ resolved.

The phonon wake structure in our MD simulation was in general similar to that observed in the experiment and predicted by theory. The simulation revealed the same elements of the wake structure: Mach cones composed of compressional and shear waves, supersonic and subsonic lateral wakes, and subsonic transverse wakes. They appeared at the same excitation speeds and had comparable opening angles. The similarity of the phonon wakes in our simulation and experiment demonstrates that the simulation incorporated the essential physics of the experiment.

Neither our experiment nor our simulation revealed the criss-cross wake of umklapp phonons predicted by the theory of Ref. [12]. Unlike the Mach cones and lateral wakes at larger opening angles, the umklapp wake is sensitive to the lattice orientation angle Θ, whereas the results of our simulation and experiment are Θ averaged. Thus, we attribute the lack of the criss-cross signature of umklapp phonons to our averaging method. This averaging method, however, does not obscure the Mach cone, lateral wake, or transverse wake.

The results of our MD simulation, because they have much in common with the experiment but without its limited field of view, lead us to suggest an explanation of a previously mentioned difference, between theory and experiment, in the shapes of wakes. The theory of Ref. [12], which assumes that the moving disturbance began long ago and far away, predicts only an outward bending of the lateral wake's wings, as in Fig. 9(e). However, in our experiment the wings bend outwards near the apex, and then inwards at a longer distance, as in Fig. 9(c). In the experiment, the moving disturbance began not at infinity, but at a location within the finite-sized lattice. In Fig. 14(a) we show the simulation results for a compressional wake using parameters similar to the experimental parameters of Fig. 8(c). As in the experiment, the simulated laser spot was at first pointed at the location marked by a cross in Fig. 14(a), and then the spot started to move. This yielded not only a lateral wake, but also a system of concentric circular wave fronts centered around the location where the laser spot began. These circular wave fronts are caused by the momentary pointlike dis-

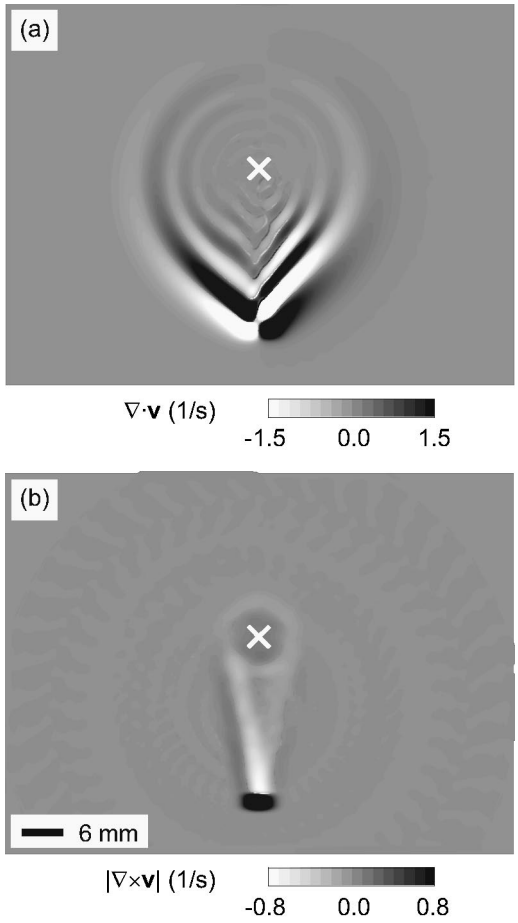

FIG. 14. A MD simulation assuming a Yukawa interparticle potential and parameters similar to those of Fig. 8. The maps are shown for (a) divergence of the particle velocity $\nabla \cdot \mathbf{v}$ and (b) vorticity $|\nabla \times \mathbf{v}|$. (a) The compressional waves form a Mach cone followed by multiple lateral wakes, all of them smoothly connected to a system of concentric circular wave fronts centered around the point where the motion of the laser spot started, marked by $\times$. This structure is explained by the dispersion of compressional waves. (b) The shear waves form only a Mach cone connected to a single circular wave front, because they are almost dispersionless.

turbance created when the laser beam first struck the lattice. The presence of more than just one circular wave front is explained by the dispersion of compressional waves [36]. The shear waves, on the other hand, have little dispersion, and they form only one such wave front, connected to a Mach cone, as shown in Fig. 14(b). For the compressional waves, the smooth transition between each wing of the lateral wake and its corresponding circular wave front corresponds to the inward bending of the wake's wings far from the apex. This behavior is a result of the finite distance traveled by the laser spot in our experiment and MD simulation. In the experiment, the camera's field of view did not include all of the circular wave fronts. The simulation, on the other hand, shows the entire lattice, and the resulting images in Fig. 14(a) lead us to an explanation for the inward curvature in the experiment: the curvature corresponds to the circular wave fronts due to the initial disturbance when we began moving the laser spot.

Another feature of the circular wave fronts in the simulation is their intensity, which is not uniform with respect to angle. This observation from Fig. 14(a) is consistent with our previous observation [36] of a distribution that is typical for a pulsed dipole source. Such a source consists of both compressional and shear waves.

An additional contribution to the inward bending of the wake's wings could arise from the nonuniform particle number density n in both our experiment and simulation. The theoretical wakes were derived assuming that n is uniform, while in the experiment and simulation, due to the bowl-shaped external confining potential, n was higher in the center of our plasma crystal and gradually declined towards its periphery. Because the sound speed increases with n (for example, at long wavelengths, $C_L \propto \sqrt{n}$ [13]), C_L is smaller at the lattice's periphery. Equation (1) predicts that this would result in a smaller opening angle for the Mach cone at the lattice's periphery, which would tend to bend the wake inwardly.

B. Test for nonlinear effects

We carried out a test using our MD simulation to reveal how nonlinearity in the vicinity of the excitation spot can affect the (linear) far-field wake structure. A nonlinearity in the near field arises due to the high speed v attained by particles within the excitation spot, as high as $v = (0.12\text{–}0.23)C_L$ depending on the scanning speed. In a previous experiment with laser-excited pulses under similar experimental conditions, it was found that the effect of nonlinearity became obvious for $v > 0.07C_L$ [33].

Our experimental wakes are asymmetric, that is, their left-hand side is different from their right-hand side (RHS), as shown in the particle-speed map in Fig. 15(a). The wake asymmetry stems from the asymmetry of the excitation technique, where the laser beam strikes the lattice from the RHS. The linear theory of Ref. [12], however, predicts a symmetric particle-speed distribution in the wake shown in Fig. 15(b), even for the asymmetric-excitation technique. This leads us to an assumption that the asymmetry of the experimental speed map in Fig. 15(a) is caused by nonlinearity that is one of the main differences between our experiment and the theory of Ref. [12].

We tested the assumption that nonlinearity explains the asymmetry of the experimental wake, using our MD simulation. We repeated the MD simulation in two ways, first using the usual Yukawa interparticle potential and thereby retaining nonlinear effects, and then using an interparticle potential that was linearized so that forces were exactly proportional to particle displacement. Otherwise, the parameters were chosen to be similar to the experimental conditions in Fig. 15(a). The simulation retaining nonlinear effects yielded an asymmetric wake structure shown in Fig. 15(c) that is similar to the experimental wake. The simulation with a linearized interaction, on the other hand, yielded a symmetric wake structure, shown in Fig. 15(d), that is similar to the linear theoretical wake in Fig. 15(b). This comparison demonstrates that the asymmetry of the wake is due to nonlinear effects.

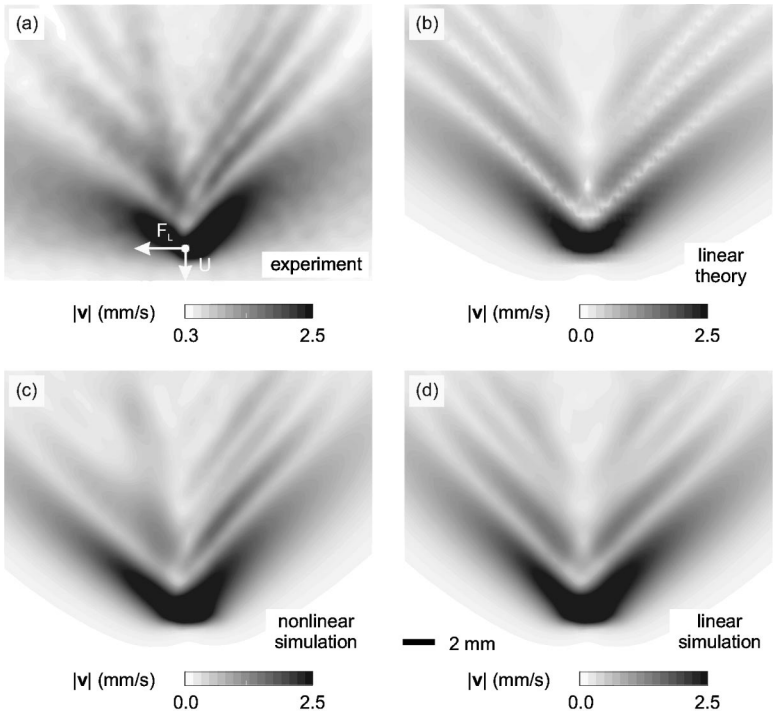

FIG. 15. The role of nonlinearity in the wake's asymmetry. The maps show the particle speed v for (a) the experimental wake of Fig. 8(a), (b) linear theoretical wake predicted by the theory of Ref. [15], (c) the results of a MD simulation with a Yukawa interparticle potential, and (d) the results of a MD simulation with a linearized interparticle potential. The parameters are similar to those of Fig. 8. The linear wakes in (b) and (d) are symmetrical; the asymmetry of the wakes in (a) and (c) is caused by nonlinearity in the vicinity of the excitation spot.

These nonlinearities are localized in the near field, yet the wake in the far field is also asymmetric. This can be explained simply because the waves in the far field originated in the near field. Waves in the far field are linear, and for this reason we used only the wake structure in the far field when calculating the compressional wave's dispersion relation in Fig. 13.

VII. SUMMARY

We observed and measured the phonon wakes formed by compressional and shear waves in a 2D screened-Coulomb crystal. Our experimental system was a 2D dusty plasma crystal, arranged in a triangular lattice with a repulsive interparticle potential. The wakes were excited by a moving spot of the Ar^+ laser light.

The experimentally observed phonon wakes agreed in the far field with the linear theory of Ref. [12] and a 2D MD simulation, both of which assume a Yukawa interparticle potential. We observed additional types of phonon wakes predicted by the theory of Ref. [12], the subsonic lateral and transverse wakes, which were not previously reported in dusty plasma experiments. The phonon wake structure is explained by the dispersive properties of the constituent waves.

We developed a generally useful technique of calculating the dispersion relation of compressional waves, based on the analysis of the spatial structure of phonon wakes created by a moving disturbance, according to the theory of Ref. [12]. An advantage of this technique is that a single snapshot of the wake is sufficient to calculate the dispersion relation in a wide range of wave numbers. By fitting the experimentally measured dispersion relation to a theoretical dispersion relation assuming a particular interparticle potential, it is possible to characterize the potential. For our plasma crystal, this method yielded values of the screening parameter κ and particle charge Q that agreed with those obtained by other methods.

ACKNOWLEDGMENTS

We thank A. Bhattacharjee and S. Nunomura for helpful discussions and L. Boufendi for TEM measurements. Work at Iowa was supported by NASA, NSF, and the U.S. Department of Energy. D.H.E.D. acknowledges support from the NSF (Grant No. PHY-9876999) and ONR (Grant No. N00014-96-1-0239). A.P. acknowledges the DFG for supporting his sabbatical leave under Grant No. Pi185/21-1.

[1] N. Cheng, Zh. Zhu, C.H. Cheng, and M.N. Toksöz, Geophys. Prospect. **42**, 303 (1994).
[2] P. Gumbsch and H. Gao, Science **283**, 965 (1999).
[3] J.H. Chu and I. Lin, Phys. Rev. Lett. **72**, 4009 (1994).
[4] H. Thomas *et al.*, Phys. Rev. Lett. **73**, 652 (1994).
[5] Y. Hayashi and K. Tachibana, Jpn. J. Appl. Phys., Part 2 **33**, L804 (1994).
[6] A. Melzer, T. Trottenberg, and A. Piel, Phys. Lett. A **191**, 301 (1994).
[7] U. Konopka, G.E. Morfill, and L. Ratke, Phys. Rev. Lett. **84**, 891 (2000).
[8] A. Homann *et al.*, Phys. Rev. E **56**, 7138 (1997).
[9] F. Behroozi, Langmuir **12**, 2289 (1996).
[10] F.M. Peeters and X. Wu, Phys. Rev. A **35**, 3109 (1987).
[11] R.S. Crandall, Phys. Rev. A **8**, 2136 (1973).
[12] D.H.E. Dubin, Phys. Plasmas **7**, 3895 (2000).

[13] X. Wang, A. Bhattacharjee, and S. Hu, Phys. Rev. Lett. **86**, 2569 (2001).
[14] P.K. Kaw and A. Sen, Phys. Plasmas **5**, 3552 (1998).
[15] M.S. Murillo, Phys. Rev. Lett. **85**, 2514 (2000).
[16] M. Rosenberg and G. Kalman, Phys. Rev. E **56**, 7166 (1997).
[17] G. Kalman, M. Rosenberg, and H.E. DeWitt, Phys. Rev. Lett. **84**, 6030 (2000).
[18] J.B. Pieper and J. Goree, Phys. Rev. Lett. **77**, 3137 (1996).
[19] A. Homann, A. Melzer, S. Peters, R. Madani, and A. Piel, Phys. Lett. A **242**, 173 (1998).
[20] S. Nunomura, J. Goree, S. Hu, X. Wang, and A. Bhattacharjee, Phys. Rev. E **65**, 066402 (2002).
[21] S. Nunomura, D. Samsonov, and J. Goree, Phys. Rev. Lett. **84**, 5141 (2000).
[22] H. Ohta and S. Hamaguchi, Phys. Rev. Lett. **84**, 6026 (2000).
[23] O. Havnes, T. Aslaksen, T.W. Hartquist, F. Li, F. Melandsø, G.E. Morfill, and T. Nitter, J. Geophys. Res. **100**, 1731 (1995).
[24] O. Havnes, F. Li, T. Aslaksen, T.W. Hartquist, G.E. Morfill, T. Nitter, and V. Tsytovich, J. Vac. Sci. Technol. A **14**, 525 (1996).
[25] A. Brattli, O. Havnes, and F. Melandsø, Phys. Plasmas **9**, 958 (2002).
[26] D. Samsonov *et al.*, Phys. Rev. Lett. **83**, 3649 (1999).
[27] D. Samsonov, J. Goree, H.M. Thomas, and G.E. Morfill, Phys. Rev. E **61**, 5557 (2000).
[28] A. Melzer *et al.*, Phys. Rev. E **62**, 4162 (2000).
[29] V. Nosenko, J. Goree, Z.W. Ma, and A. Piel, Phys. Rev. Lett. **88**, 135001 (2002).
[30] Z.W. Ma and A. Bhattacharjee, Phys. Plasmas **9**, 3349 (2002).
[31] B. Liu, J. Goree, V. Nosenko, and L. Boufendi, Phys. Plasmas **10**, 9 (2003).
[32] S. Hamaguchi, R.T. Farouki, and D.H.E. Dubin, Phys. Rev. E **56**, 4671 (1997).
[33] V. Nosenko, S. Nunomura, and J. Goree, Phys. Rev. Lett. **88**, 215002 (2002).
[34] Th. Trottenberg, A. Melzer, and A. Piel, Plasma Sources Sci. Technol. **4**, 450 (1995).
[35] S. Nunomura, J. Goree, S. Hu, X. Wang, A. Bhattacharjee, and K. Avinash, Phys. Rev. Lett. **89**, 035001 (2002).
[36] A. Piel, V. Nosenko, and J. Goree, Phys. Rev. Lett. **89**, 085004 (2002).
[37] W.H. Munk, P. Scully-Power, and F. Zachariasen, Proc. R. Soc. London, Ser. A **412**, 231 (1987).